Microfluidics and Nanofluidics (2019) 23:37
https://doi.org/10.1007/s10404-019-2206-1

RESEARCH PAPER

Polymeric fully inertial lab-on-a-chip with enhanced-throughput sorting capabilities

Annalisa Volpe[1] · **Petra Paiè**[2] · **Antonio Ancona**[1] · **Roberto Osellame**[2,3]

Received: 1 November 2018 / Accepted: 7 February 2019

Abstract
In biology and medicine, the application of microfluidics filtration technologies to the separation of rare particles requires processing large amounts of liquid in a short time to achieve an effective separation yield. In this direction, the parallelization of the sorting process is desirable, but not so easy to implement in a lab on a chip (LoC) device, especially if it is fully inertial. In this work, we report on femtosecond laser microfabrication (FLM) of a poly(methyl methacrylate) (PMMA) inertial microfluidic sorter, separating particles based on their size and providing an enhanced-throughput capability. The LoC device consists of a microchannel with expansion chambers provided with siphoning outlets, for a continuous sorting process. Different from soft lithography, which is the most used technique for LoC prototyping, FLM allows developing 3D microfluidic networks connecting both sides of the chip. Exploiting this capability, we are able to parallelize the circuit while keeping a single output for the sorted particles and one for the remaining sample, thus increasing the number of processed particles per unit time without compromising the simplicity of the chip connections. We investigated several device layouts (at different flow rates) to define a configuration that maximizes the selectivity and the throughput.

Keywords Lab on a chip · Fs-Laser micromachining · Inertial sorting · Microfabrication · PMMA

1 Introduction

Isolating and sorting cells from complex and heterogeneous mixtures represent a critical task in many areas of biology, biotechnology, and medicine. Cell sorting is often used to enrich or purify cell samples into well-defined populations or for the isolation from blood of rare target cell populations, including circulating tumor cells (CTCs) (Cho et al. 2018; Rana et al. 2018; Vona et al. 2000) and circulating fetal cells (CFCs) (Gänshirt et al. 1998). Meanwhile, the growing interest in personalized medicine, in which treatments are tailored to the prognoses of patients, is always growing.

Microfluidics, the science and technology of controlling and manipulating fluids at volumes on the order of microliters, has received considerable attention in recent years for sorting micro-particles. Some of the promising advantages of microfluidic systems, also called lab on a chip (LoC), include reduced sample volume, automatic sample processing and high efficiency. The reduced sample volume, however, may be a limitation when rare cells have to be sorted. In such cases, it is important to increase the throughput of these devices without affecting the purity of the sorted sample (Bhagat et al. 2011; Guo et al. 2012).

Polymeric materials are considered the best choice for LoC fabrication: they are cheap, bio-compatible, nontoxic, transparent and permeable to gases. Furthermore, cost-effective fabrication processes for polymeric LoC are available, i.e., soft lithography (Kim et al. 2008), thermoforming (Heckele and Schomburg 2004) and micro-injection moulding (Trotta et al. 2018; Vázquez et al. 2017). To determine which fabrication technology is the best suited, it is important to take into account the choice of the material substrate, the production costs and manufacturing time, as well as the chip design and the desired functions to integrate (Becker and Gärtner 2008).

Annalisa Volpe and Petra Paiè contributed equally to this work.

✉ Annalisa Volpe
annalisa.volpe@ifn.cnr.it

[1] Institute for Photonics and Nanotechnologies (IFN)-CNR, Via Amendola 173, 70126 Bari, Italy

[2] Institute for Photonics and Nanotechnologies (IFN)-CNR, Piazza Leonardo da Vinci 32, 20133 Milan, Italy

[3] Department of Physics, Politecnico di Milano, Piazza Leonardo da Vinci 32, 20133 Milan, Italy

Published online: 13 February 2019

The microfluidic sorting techniques can be classified into two categories: passive methods in which the functionality is established by exploiting geometrical effects and/or hydrodynamic forces in the microchannel (Karimi et al. 2013); active methods, such as dielectrophoresis (Chan et al. 2018), magnetophoresis (Liu et al. 2016), and acoustophoresis (Simon et al. 2017), which are based on the application of external force fields. Active microfluidic systems ensure high separation efficiency but require sophisticated external controls. Contrary to active approaches, the passive microfluidic techniques [such as deterministic lateral displacement (Holm et al. 2011; McGrath et al. 2014), hydrodynamic filtration (Davis et al. 2006), and pinched flow fractionation (Yamada et al. 2004)] rely exclusively on the intrinsic hydrodynamics to separate the microparticles, thus greatly simplifying the design, fabrication and operation of the devices. Other advantages of passive sorting methods are the label-free operation and the unaffected viability of living particles, despite a lower separation efficiency as compared to the active ones.

Recently, it has been shown that particles flowing through microchannels of various geometries, including straight (Wang et al. 2015; Wu et al. 2016), curved (Bayat and Rezai 2018), spiral (Bhagat et al. 2008; Paiè et al. 2017a), and serpentine channels (Zhang et al. 2014a, b), can migrate towards distinct positions across the streamlines, due to the onset of inertial forces whose intensity is highly dependent on the particle dimension (Amini et al. 2014; Zhang et al. 2016). This occurs only when the Reynolds number ($Re = ud/\nu$, where u is the fluid average velocity, d is a characteristic channel dimension, and ν is the fluid kinematic viscosity) is between 1 and 100. We refer to this intermediate range, between Stokes and turbulent regimes, as inertial microfluidics.

Inertial focusing was initially discovered by Segre and Silberberg in a circular tube (Segre and Silberberg 1961), and then proved in channels with square cross sections (Chun and Ladd 2006; Kim and Yoo 2008). However, among all, microfluidic channels with rectangular cross sections have received the greatest attention in the literature due to their ease of fabrication and to the fact that high aspect ratio sections reduce the number of equilibrium positions to only two, located near the widest faces of the channel (Bhagat et al. 2009).

The inertial migration effect in rectangular cross-sectional channel was exploited by Sollier et al. (2014) to passively isolate larger cells while smaller cells were flushed out of the device. They tailored a polydimethylsiloxane (PDMS) chip specifically for the high-purity extraction of cancer cells from blood samples and assessed its performance. The microfluidic device consisted of straight microchannels (to pre-focus the cells), followed downstream by multiple expansions (microchamber) placed in series and parallel.

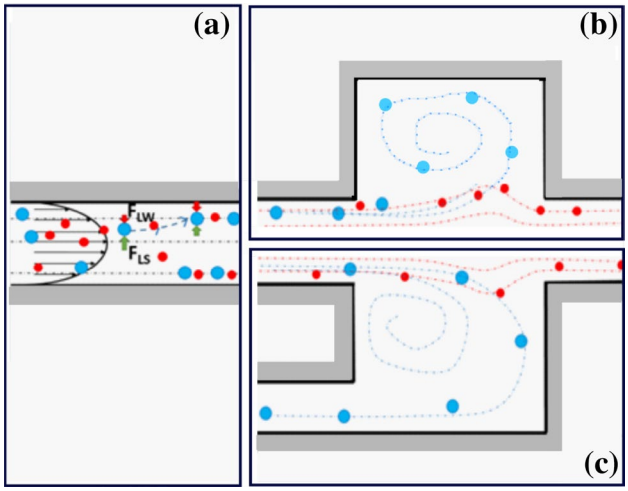

Fig. 1 Schematic representation of the inertial sorting of neutrally buoyant particles flowing in a straight wall-bounded Poiseuille flow with expansion and lateral outlets. **a** At the inlet of the channel, the randomly distributed particles undergo two opposite lift forces: the wall-induced lift force FLW, which directs the particles away from the wall and the shear gradient induced lift force FLS, which directs the particles away from the channel center. As a result, the particles migrate to lateral equilibrium positions. **b** At the entrance of the chamber the larger particles (blue) are subjected to a larger FLS that pushes them towards the reservoir, allowing a separation from the smaller ones (red) that flow towards the outlet, with a negligible lateral migration. **c** The presence of a lateral siphoning outlet allows a continuous extraction of the larger particles from the reservoirs. (Color figure online)

The working principles of the device are illustrated in Fig. 1 a, b.

The neutrally buoyant particles flowing in the straight channel are subjected to two opposing inertial forces (Amini et al. 2014): (1) the wall-induced lift force (F_{LW}), originated by the disturbance of the wall on the flow field around near-wall particles and directing the particles away from the wall; (2) the shear gradient induced lift force (F_{LS}), caused by the curvature of the undisturbed fluid velocity profile and directing the particles away from the channel center. These two opposite forces find a balance in well-determined equilibrium positions, which depend on the geometry of the microchannel cross section. In the expansion chamber, under particular flow conditions and microchamber dimensions, particles larger than a defined cut-off size can be selectively trapped in microscale vortices, while smaller particles are flushed out of the device. After a washing step that removes any remaining small particle, the larger ones are released by simply lowering the flow rate. This last step can be avoided by adding to the microchamber siphoning outlets for continuous inertial separation (Fig. 1c), as shown by Wang and Papautsky (2015). This improvement of the original device design also reduces the vortex instabilities originated by the continuous interactions between the particles already

trapped and the newcomers, which is one of the main causes for the loss of trapped cells in the vortex based design (Paiè et al. 2017b). Furthermore, Wang and Papautsky demonstrated that the cut-off diameter of the particles trapped in the microchamber can be precisely tuned by modifying the resistance of the outlet channels.

The 2D nature of soft lithography shows its intrinsic limitations when the complexity of the manufacturing devices increases. Indeed, with this fabrication technique, it is not possible to parallelize the design proposed by Wang and Papautsky (2015) without increasing the number of required fluidic connections. Practically, this prevents the possibility to increase the device throughput, which is a real necessity for rare cells sorting, thus vanishing the advantages of the siphoning outlets. This poses a severe limitation to this approach, which would indeed be beneficial for numerous applications in biology and medicine (i.e., disease diagnosis, genetic analysis, drug screening and therapeutic) where it is required to process a large amount of liquid in the shortest possible time. In this direction, the parallelization of the fully inertial sorting process is crucial, but not so easy to implement into a single device with the existing microfabrication technologies. At the best of our knowledge, an enhanced throughput with high-purity samples has been achieved only by combining the inertial sorting with other techniques. Nivedita et al. (2017) exploited a passive spiral inertial microfluidic device with an active lateral cavity acoustic transducer. They demonstrated that this platform is capable of efficiently (> 90%) removing smaller cells in a heterogeneous cell line. Bhagat et al. (2011) introduced a high-throughput size-based separation method for processing diluted blood using inertial microfluidics, coupled with pinched flow dynamics for isolating low-abundance cells from blood. Results from experiments conducted with MCF-7 cells spiked into whole blood indicate > 80% cell recovery.

In this paper, we propose to exploit femtosecond-laser micromachining technology (FLM) to develop a polymeric 3D inertial microfluidic sorter, discriminating particles on the basis of their size and operating continuously, without the 'wash and release' step. As a non-clean room process, FLM provides a convenient, economical and flexible way to fabricate microfluidic patterns by varying the laser parameters (Farson et al. 2008). Moving the beam, designs are directly transferred from a computer file to the device, thus avoiding the expensive and time-consuming production of masks. Furthermore, FLM enables an energy deposition at a shorter timescale than the electron–phonon coupling processes, which allows the material to be removed by laser ablation from the irradiated area with negligible thermal damage to the surrounding substrate (Kononenko et al. 1999). In this way, it is possible to create micromilled features with high precision and resolution (Sima et al. 2018) almost completely free of thermally induced defects like surface or subsurface cracks, residual stresses, resolidified melting and burrs, the latter being very problematic for the assembly and sealing of the LoC. Therefore, for rapid prototyping of polymeric LoC, FLM is more suitable than the conventional micromilling technology, which suffers from limited resolution and surface quality due to the size of the milling tool.

In addition, FLM does not pose any restriction on the type of polymer to be used. Therefore, poly(methyl methacrylate) (PMMA) has been chosen as a substrate material for our devices since it is biocompatible, transparent and more rigid than PDMS. The latter is the most used polymer for LoC production by soft lithography. However, PDMS is not the best choice for applications where it is required to withstand high liquid pressures. In fact, because of its softness, the risk that the deformations of the microchannel will change the flow behavior along the chip (Gervais et al. 2006), leading to ambiguous results (Cheung et al. 2012; Hardy et al. 2009), is very high.

Taking advantage of the great flexibility of FLM, a multichannel device is fabricated, with the aim of enabling the parallelization of the sorting process and improving the throughput of current implementations (Volpe et al. 2017; Wang and Papautsky 2015), while keeping the sorting efficiency. Being more specific, the microfluidic devices presented in this paper consist of microchannels with periodic expansion chambers, which are upgraded with siphoning outlets leading to the backside of the chip. Several devices with varying number of chambers and different collecting geometries (at different flow rates) are investigated, aiming to find the layout with maximized trapping efficiency and enhanced throughput.

The overall organization of the paper is as follows: the next section introduces the fs-laser fabrication and the sorting characterization methods; in the subsequent section the different device designs are described, and the experimental results are presented and discussed.

2 Materials and methods

2.1 Microfluidic device fabrication

The microfluidic devices were fabricated on 1-mm-thick PMMA layers (Vistacryl CQ, Vista Optics Ltd) by femtosecond-laser milling.

We used an ultrafast fiber laser system (mod. Trumpf TruMicro Femto Edition) delivering 900-fs pulses at a wavelength of 1030 nm with an almost diffraction limited beam ($M^2 < 1.3$), repetition rate varying from 1 to 800 kHz, maximum pulse energy of 400 μJ and maximum average

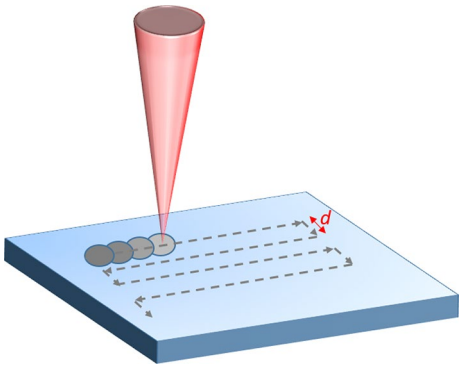

Fig. 2 Schematic diagram of the laser scanning path for milling; *d* is the distance between adjacent parallel lines of the hatch scanned by the laser. The laser spot has a diameter of about 20 µm

Table 1 Laser milling parameters

E_p (µJ)	Repetition rate (kHz)	Scan speed (mm/s)	Hatch (µm)	Loop #
8	25	30	3	2

power of 40 W. The circularly polarized laser beam was focused and moved onto the target surface by a galvo scan head (mod. IntelliSCANN 14, SCAN-LAB, Puchheim, Germany) equipped with an f-theta telecentric lens of 100 mm focal length.

The fs-laser milling process was carried out by removing the material layer by layer according to the LoC design. The ablation depth was carefully controlled by adjusting the number of scanning loops.

Preliminary fs-laser milling tests have been carried out to find the best combination of process parameters, namely the pulse energy, the scan speed, the spacing of the hatch *d* (Fig. 2) and number of scanning loops, to get the desired depth.

Based on the results of the preliminary tests, the laser parameters reported in Table 1 have been used for the fabrication of the LoC devices. The milling process was carried out on the two faces of the PMMA sheet to obtain complex 3D fluidic networks with channels that connect the two faces. First, the fluidics was micromilled on the upper side of the sample, then, with the aid of a camera, the sample was turned on the other side and the inlet and outlet holes and the collecting chamber (if present) were micromachined.

After the laser process, loosely attached debris was removed by ultrasonic cleaning in distilled water for 10 min. The dimensions of the fs-laser milled micro-features were measured by an optical microscope (Nikon Eclipse ME600). Moreover, the average roughness Ra of the milled surface was measured by means of an optical ContourGT InMotion profilometer with nanometric resolution and was estimated to be <2 µm. This value is negligible compared to the channel height; therefore, we believe that the roughness is not affecting the fluidics of the particle sorting process.

In Fig. 3a, an example of the fabricated microfluidic network is shown. A detail of a microchamber (highlighted with dark line in Fig. 3a) is magnified in Fig. 3b. In Fig. 3c a, microscope image of a 50-µm-wide channel is further shown. Here, it is possible to note the absence of resolidified burrs and fairly regular edges, typical of an FLM process. The size of the channel and chamber shown in Fig. 3b, c matches with high precision the designed dimensions (see Table 2).

2.2 Testing of the devices

After the laser milling step described in the previous section, the microfluidic network engraved on the PMMA surfaces had to be sealed. The devices were sealed using a pressure sensitive transparent tape (Absolute QPCR seal), that is optically clear, transparent to fluorescence transmission and non-sticky. The transparent tape is used in correspondence to the ablated structures. Considering that our device design presents three-dimensional channels, milled on both sides of the PMMA substrate, we positioned the tape both on the top and bottom surfaces. Subsequently, PEEK tubes from IDEX were inserted and glued to the access holes fabricated in the

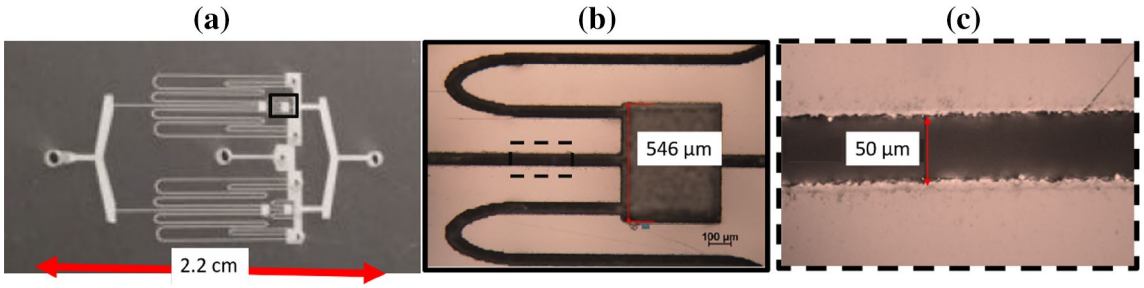

Fig. 3 **a** Top view image of a microfluidic network machined on the PMMA substrate; the detail of a microchamber is highlighted in the black square. **b** Optical microscope image of the microchamber with inlet and outlet channels; the dark dashed line surrounds a part of the inlet microchannel, which is magnified in **c**

Table 2 Main dimensions of the one-chamber LoC cell sorter

	Length (mm)	Height (μm)	Width (μm)
In ($L_{in} \times H \times W_{in}$)	7	60	50
Out ($L_{out} \times H \times W_{out}$)	1	60	50
$Lat_{1,2}$ ($L_{lat} \times H \times W_{lat}$)	30	60	50
Microchamber ($L_{ch} \times H \times W_{ch}$)	0.480	60	540

substrate to allow an easy sample delivery and collection. The tubes had external and internal diameters equal to 0.78 and 0.5 mm, respectively. The device characterizations were performed using separately 6- and 15-μm fluorescent beads from Sigma-Aldrich and Phosphorex, respectively, whose dimensions mimic the red blood cells and the CTC ones. Two solutions were prepared, one of about 4.35×10^5 beads/ml for the smaller beads, and a second one of about 2×10^4 beads/ml for the larger beads. The sample was inserted at well-defined flow rates by means of a high-pressure syringe pump (KDS410, from KDScientific). Sample droplets exiting from the outlets (both from the main and the lateral ones) were collected in a multi-well plate. The wells were subsequently imaged with a fluorescent microscope and analyzed with ImageJ to count the number of beads contained in each well. The liquid collection was performed paying attention to accumulate the same amount of liquid (i.e., the number of droplets) from all the outlets to facilitate a direct comparison of the population and to determine the efficiency and the purity of each device (i.e., the percentage of large beads that flow towards the lateral outlet and the percentage of small beads that flow towards the main outlet). Each measurement was performed at least three times to average the results.

3 Results and discussion

3.1 Design of the inertial LoC sorter

The design of the device was based on the principle described in "Introduction" and explored by Wang and Papautsky (2015): a straight microchannel pre-focuses the cell, which is sorted in the following chamber depending on their size due to imbalanced lift forces. The siphoning outlets allow continuous cell sorting. The strategy was to increase the number of chambers put in series and in parallel to proportionally increase the device selectivity and the throughput, respectively. In particular, two microchambers in series aim to increase the total number of bigger particle collected by capturing in the second sorting chamber those particles that escape from the first one. Meanwhile, a two-branch device should double the throughput. At the same time, different approaches were explored to simplify the device layout for the collection of the sorted particles.

In Fig. 4a, the core of the fabricated microfluidic device with a single microchamber is sketched: a filter before the straight inlet microchannel (In) helps to avoid the channel clogging; the two lateral siphoning outlets (Lat_1, Lat_2) converge in a single tube (Lat) to simplify the connections. The main dimensions of the one-chamber device are illustrated in Fig. 4b and summarized in Table 2. They are based on the experimental results of Sollier et al. (2014) and Volpe et al. (2017). Figure 4c shows a microscope image acquired while flowing fluorescent particles in the device.

The length of the inlet was set considering the minimum value required for focusing particles at the lowest flow rate studied (Amini et al. 2014). The length of the outlets and the chamber dimensions have been determined by previous simulation and experimental work (Volpe et al. 2017) to ensure at $Re = 100$ (flow rate ~25 ml/min) an efficient sorting of 15 μm particle from 6 μm ones.

After the one-chamber LoC, a device consisting of two microchambers in series was fabricated. The characteristic dimensions of the chip with two chambers in series are listed in Table 3.

In Fig. 5a, b, a two-branch device consisting of four chambers, with and without a collecting circuit, is sketched. The collecting circuit in Fig. 5a, machined by laser ablation on the other side of the polymer plate, is connected to the

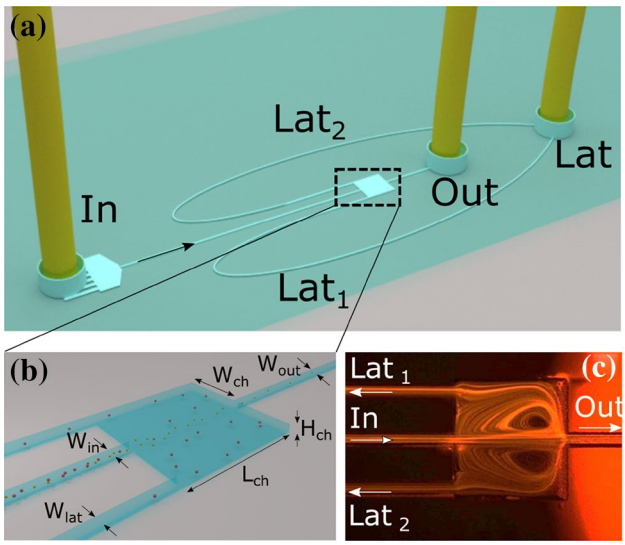

Fig. 4 **a** Sketch of the single-chamber chip, with **b** a detail of the reservoir where the fundamental dimensions are labelled and the operating mechanism is schematically represented: the larger particles are siphoned out from the lateral outlets when the optimized flow rate is reached. **c** Fluorescent microscope image of the real device acquired with beads of 6 μm, at a fluid flow rate of 0,6 ml/min. In the chamber, the inlet flow is split into the main and lateral flow components, exiting from the corresponding outlets. Vortices occur in the chamber. Here the particles are trapped, before exiting through $Lat_{1,2}$

Table 3 Main dimensions of the two-chamber chip

	Length (mm)	Height (μm)	Width (μm)
In ($L_{in} \times H \times W_{in}$)	7	60	50
Out_1 ($L_{out} \times H \times W_{out}$)	1	60	50
Out_2 ($L_{out} \times H \times W_{out}$)	0.500	60	50
Lat_1 ($L_{lat} \times H \times W_{lat}$)	30	60	50
Lat_2 ($L_{lat} \times H \times W_{lat}$)	11.5	60	50
$Microchamber_{1-2}$ ($L_{ch} \times H \times W_{ch}$)	0.480	60	540

$Outlet_1$ is also the inlet of the second chamber

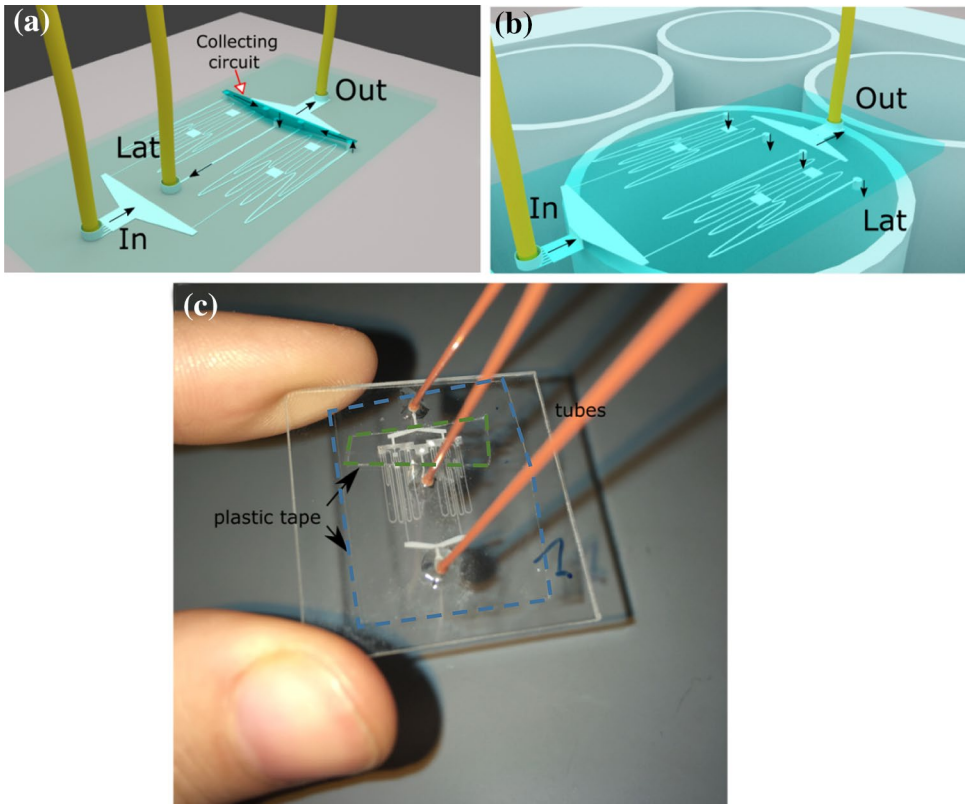

Fig. 5 Schematic illustration of the four-chamber device. The flow exiting from the siphoning outlets is collected **a** by a single tube (Lat), which receives the collected sample from all the lateral channels through the "collecting circuit" fabricated on the other side of the chip or **b** directly in a multi-microwell plate. Black arrows indicate the flowing direction of the fluid. **c** A picture of the device illustrated in panel a, with the tubes for inlet and outlet and lateral collection. The plastic tapes used to seal the chip on the upper and bottom PMMA surfaces are indicated by black arrows and are highlighted with a blue and green dashed contour, respectively. (Color figure online)

upper microfluidic network and to the outlet tube by means of two laser-drilled holes. In this layout, the circuit collecting the bigger particles is directly connected to a microfluidic tube, thus gathering in a single microfluidic outlet all the particles sorted in the different chambers. Alternatively, the layout presented in Fig. 5b collects the drops coming out from the lateral outlets directly in the multi-well plate with no tubes. This can increase the simplicity of the measurements, facilitating the experiments. Figure 5c shows a picture of a device completely assembled. The design corresponds to the scheme shown in Fig. 5a with inlet, outlet and lateral tubes. Plastic tape is used to seal both the substrate surfaces.

3.2 Device characterization

As a first step, we explored the possibility to add multiple chambers in series. The sorting efficiency of the device made by a single chamber (Fig. 4) was compared with the efficiency of the device made by two chambers in series, placed along the same straight channel. Figure 6 shows the results of a typical device characterization. It reports the comparison between the populations collected from the lateral and from the outlet tubes using the single chamber device. In this case, 15- and 6-μm beads were processed in the device at a flow rate of 0.3 ml/min. It is possible to observe the unequal splitting of the beads depending on their size: the larger and smaller ones preferentially go towards the lateral and main outlets, respectively.

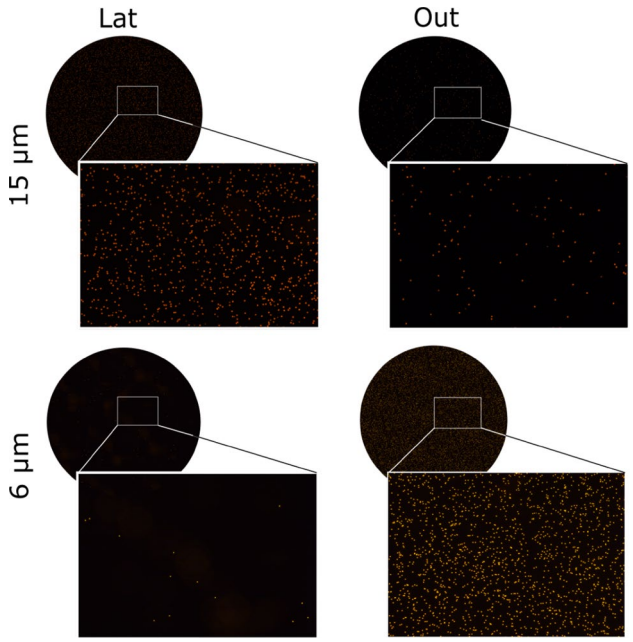

Fig. 6 Fluidic characterization of the device with a single reservoir at 0.3 ml/min. The bigger particles are preferentially collected from the lateral outlets, while the smaller ones exit from the main outlet

The comparison between the performances of a single-chamber and a two-chamber device is reported in Fig. 7, where panel a shows the percentage of small beads collected from the main outlet, while panel b shows the percentage of large beads collected from the lateral outlets.

Observing the results, the flow rate that maximizes the larger bead collection is 0.3 ml/min for the device with two chambers in series. In particular, the two-chamber layout allows collecting from the lateral outlets up to 90% of the larger beads with a contamination of only 1% of small beads. However, the improvement introduced by the second reservoir is lower than expected. The reason is that the fluid flow rate entering the second reservoir is lower than the one entering the first reservoir due to the presence of the siphoning outlets. Therefore, the capturing efficiency is not constant along the device, but it decreases in the second chamber. This negative trend would become more and more severe with an increasing number of reservoirs in series. For this reason, we have not further explored the fabrication of devices with additional reservoirs in series.

We have examined the possibility to add other branches in parallel, each one constituted by two reservoirs in series. Based on the results shown in Fig. 7, each branch has to work at the optimal flow rate of 0.3 ml/min. This solution offers the further advantage of increasing the flow rate at the device input proportionally to the number of branches, thus processing a significantly higher amount of sample. As a following step, we have thus fabricated a second channel in parallel that doubles the previous layout (Fig. 5a). As a consequence, also the flow rate at the device entrance was doubled. In order to maintain a single inlet and two outlets only, as described in "Design of the inertial LoC sorter", some fluidic connections have been fabricated on the other side of the substrate with respect to the reservoirs, exploiting the unique capability of fs-laser technology. This connection channel collects the liquid from all the lateral channels redirecting it towards a single outlet.

Characterization results of the two-branch device, compared to the single-branch one, are reported in Fig. 8. As before, the percentage of small beads collected from the main outlet is shown in panel a, while panel b shows the efficiency in recovering large beads from the lateral outlets. The flow rate reported is the value per branch, which means that in case of two parallel branches a double quantity of sample has been processed. Unexpectedly, the two-branch device shows lower efficiency and purity. Not only the number of large beads collected from the lateral outputs is reduced, but also the number of small beads gathered from the main outlet is much lower than the single branch case. At 0.3 ml/min of flow rate, which

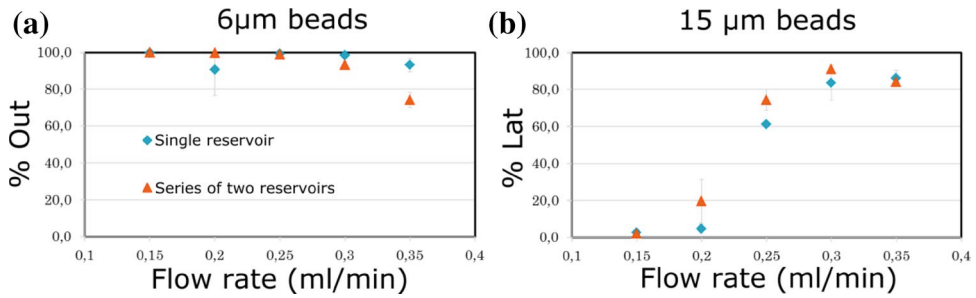

Fig. 7 Characterization of two different devices, one constituted by a single reservoir and one by two reservoirs in series. **a** The percentage of inserted small beads that that are collected from the main outlet. The value is close to 100%, which guarantees a good purity of the sample collected from the lateral outlet, and it is almost constant till 0.3 ml/min. **b** The percentage of large particles collected from the lateral outlets as a function of the flow rate The highest collection efficiency is achieved with two reservoirs in series at 0.3 ml/min

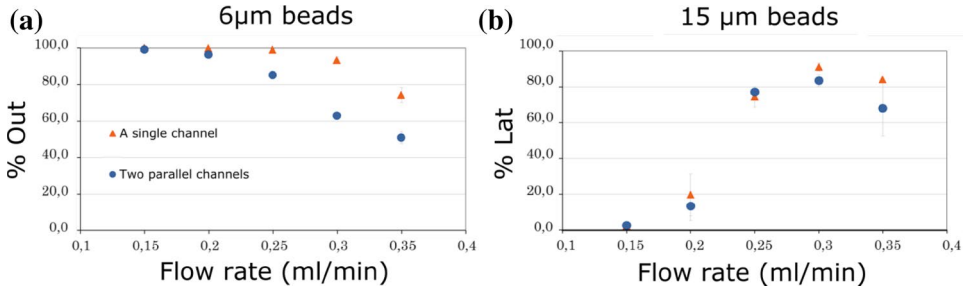

Fig. 8 Comparison between the performance of the single-branch device, and the two-branch one. **a** The characterization of the efficiency in collecting small beads from the main outlet and **b** the percentage of large beads collected from the lateral outlets. On the *x*-axis, the flow rate per single branch is reported for comparison purposes. The global flow rate of the two-branch device is double the reported value

maximizes the capturing efficiency of large beads, the percentage of small beads that are collected together with the large ones in the two-branch device is 40%, which is not acceptable if one considers that usually only tens of rare large cells are diluted among billions of red blood cells.

A possible explanation for such unexpected behavior is that the fluid flow does not split equally between the two branches. Indeed, if the fluidic resistance in the two branches is not the same, the flow rate will be divided unequally, highly affecting the device performance. The purity is particularly affected because it quickly drops down for flow rates higher than 0.3 ml/min. The main possible cause of this uneven splitting is the use of the plastic tape to seal the microfluidic network. This tape, which was applied manually, is not rigid and it deforms especially in correspondence of large channels, thus creating unequal fluidic resistances and thus unbalanced splitting of the flow rate. The larger connection channel, fabricated on the other side of the device, collecting the liquid from the lateral outlets and conveying it to the single outlet, is more prone to this kind of defect. Therefore, a further device has been fabricated where this collection channel has been eliminated as well as the lateral outlet tubes, aiming at simplifying the device layout.

A drawing of this simplified two-branch device is illustrated in Fig. 5b. Here, the lateral outlets can directly drip in a multi-well plate, so that it is possible to position the device directly above the collecting well. The possibility to avoid the output tube not only simplifies the collection procedure, but also reduces the loss of the sorted sample due to adhesion to the tube inner walls. Results from this last device are reported in Fig. 9 and compared to the single-branch device. It can be noticed that (1) the two-branch device exhibits the maximum capture efficiency of large beads at a higher flow rate of 0.4 ml/min per channel. This shift is ascribed to the different fluidic resistance of the circuit due to the absence of the tubes. (2) Comparing the two devices at their best operating point, we observe that the efficiency and the purity are very similar, proving the possibility to efficiently increase the throughput of the device by adding multiple parallel branches, without compromising the performance. In addition, this approach has the advantage of collecting the sorted sample directly in a well plate, where it can be easily analysed and further processed.

Table 4 summarizes the best results of the two devices related to the particle collection from the lateral outputs.

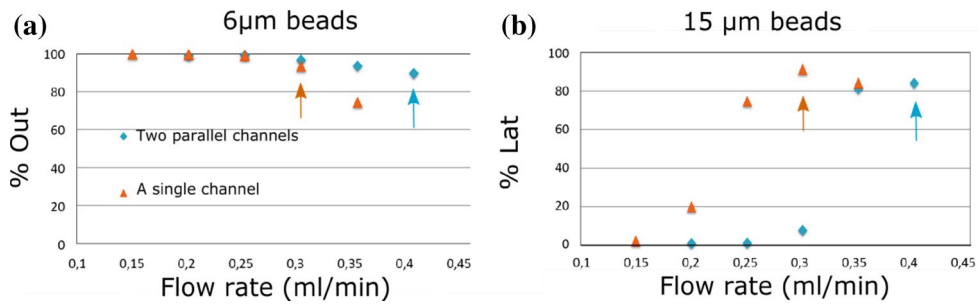

Fig. 9 Characterization of the new device with two parallel branches that drips directly in the multi-well plate compared with the single-branch one. **a, b** The characterization performed with small and large beads, respectively. On the *x*-axis, the flow rate per single branch is reported for comparison purposes. The global flow rate of the two-branch device is double the reported value. The arrows point to the results at the optimal flow rate for each device

Table 4 Percentage of small and large beads collected from LAT at the optimum flow rate

	Flow rate (ml/min)	15-μm particles %Lat	6-μm particles %(100 − out)
Single-channel device	0.3	91	4
Two-branch device	0.8	84	10

The performance of the two-branch device is still slightly worse than the single-branch one; nevertheless, it allows to process the sample at a more than double flow rate with small losses of efficiency and purity. Furthermore, we believe that a different sealing procedure could definitely solve this issue.

4 Conclusions

In this work, we exploited FLM to develop an inertial microfluidic sorter with high-throughput capability. Taking advantage of the flexibility offered by the FLM technology, complex 3D LoCs with multiple microchambers comprising siphoning outlets on the backside of the chip were fabricated. Such complex geometries cannot be produced by conventional soft lithography. In addition, FLM has no restrictions on the type of polymer to be used. Therefore, we chose PMMA as the substrate material, which is a biocompatible, transparent, thermoplastic polymer much stiffer than PDMS thus withstanding higher flowing pressures without suffering from deformations.

Our 3D cell sorter reduces the trade-off between high purity and high throughput as experienced in previous inertial size-based microfluidic devices. It offers a continuous, flow-through, single-step operation, unlike multi-step devices such as the vortex isolator (Sollier et al. 2014), providing a capture efficiency of large beads > 80%. Furthermore, this device is fully inertial, reducing the complexity of other high-throughput devices previously reported (Bhagat et al. 2011; Guo et al. 2012; Nivedita et al. 2017).

Acknowledgements The authors gratefully acknowledge the Apulian Region and the Italian Ministry of Education, University and Research (MIUR) for having supported this research activity within the projects MICROTRONIC (Lab Network cod. 71). In addition, the authors gratefully thank Francesco Bellifemine for helping during the experiments. The authors would also like to thank Professor Dino Di Carlo for the useful discussions on this topic.

References

Amini H, Lee W, Di Carlo D (2014) Inertial microfluidic physics. Lab Chip 14:2739–2761

Bayat P, Rezai P (2018) Microfluidic curved-channel centrifuge for solution exchange of target microparticles and their simultaneous separation from bacteria. Soft Matter 14:5356–5363

Becker H, Gärtner C (2008) Polymer microfabrication technologies for microfluidic systems. Anal Bioanal Chem 390:89–111

Bhagat AAS, Kuntaegowdanahalli SS, Papautsky I (2008) Continuous particle separation in spiral microchannels using Dean flows and differential migration. Lab on a chip 8:1906–1914

Bhagat AAS, Kuntaegowdanahalli SS, Papautsky I (2009) Inertial microfluidics for continuous particle filtration and extraction. Microfluid Nanofluid 7:217–226

Bhagat AAS, Hou HW, Li LD, Lim CT, Han J (2011) Pinched flow coupled shear-modulated inertial microfluidics for high-throughput rare blood cell separation. Lab Chip 11:1870–1878

Chan JY, Kayani ABA, Ali MAM, Kok CK, Majlis BY et al (2018) Dielectrophoresis-based microfluidic platforms for cancer diagnostics. Biomicrofluidics 12:011503–011521

Cheung P, Toda-Peters K, Shen A (2012) In situ pressure measurement within deformable rectangular polydimethylsiloxane microfluidic devices. Biomicrofluidics 6:026501–2650112

Cho H, Kim J, Song H, Sohn KY, Jeon MH, Han KH (2018) Microfluidic technologies for circulating tumor cell isolation. Analyst 143:2936–2970

Chun B, Ladd AJC (2006) Inertial migration of neutrally buoyant particles in a square duct: an investigation of multiple equilibrium positions. Phys Fluids 18:031704

Davis JA, Inglis DW, Morton KJ, Lawrence DA, Huang LR, Chou SY, Sturm JC, Austin RH (2006) Deterministic hydrodynamics: taking blood apart. Proc Natl Acad Sci USA PNAS 103:14779–14784

Farson DF, Choi HW, Zimmerman B, Steach JK, Chalmers JJ, Olesik SV, Lee LJ (2008) Femtosecond laser micromachining of dielectric materials for biomedical applications. J Micromech Microeng 18:035020–035028

Gänshirt D, Smeets FWM, Dohr A, Walde C, Steen I, Lapucci C, Falcinelli C, Sant R, Velasco M, Garritsen HSP (1998) Enrichment of fetal nucleated red blood cells from the maternal circulation for prenatal diagnosis: experiences with triple density gradient and MACS based on more than 600 cases. Fetal Diagn Ther 13:276–286

Gervais T, El-Ali J, Günther A, Jensen KF (2006) Flow-induced deformation of shallow microfluidic channels. Lab Chip 6:500–507

Guo MT, Rotem A, Heyman JA, Weitz DA (2012) Droplet microfluidics for high-throughput biological assays. Lab Chip 12:2146–2155

Hardy BS, Uechi K, Zhen J, Kavehpour HP (2009) The deformation of flexible PDMS microchannels under a pressure driven flow. Lab Chip 7:935–938

Heckele M, Schomburg WK (2004) Review on micro molding of thermoplastic polymers. J Micromech Microeng 14:R1–R14

Holm SH, Beech JP, Barrett MP, Tegenfeldt JO (2011) Separation of parasites from human blood using deterministic lateral displacement. Lab Chip 11:1326–1332

Karimi A, Yazdi S, Ardekani AM (2013) Hydrodynamic mechanisms of cell and particle trapping in microfluidics. Biomicrofluidics 7(2):021501–021522

Kim YW, Yoo JY (2008) The lateral migration of neutrally-buoyant spheres transported through square microchannels. J Micromech Microeng 18:065015

Kim P, Kwon KW, Park MC, Lee SH, Kim SM, Suh KY (2008) Soft lithography for microfluidics: a review. Biochip Journal 2:1–11

Kononenko T, Konov V, Garnov S, Danielius R, Piskarskas A, Tamosauskas G, Dausinger F (1999) Comparative study of the ablation of materials by femtosecond and pico- or nanosecond laser pulses. Quantum Electron 29:724–728

Liu F, Jiang L, Tan HM, Yadav A, Biswas P, van der Maarel JRC, Nijhuis CA, van Kan JA (2016) Separation of superparamagnetic

particles through ratcheted Brownian motion and periodically switching magnetic fields. Biomicrofluidics 10:064105
McGrath J, Jimenez M, Bridle H (2014) Deterministic lateral displacement for particle separation: a review. Lab Chip 14:4139–4158
Nivedita N, Garg N, Lee AP, Papautsky I (2017) A high throughput microfluidic platform for size-selective enrichment of cell populations in tissue and blood samples. Analyst 142:2558–2569
Paiè P, Bragheri F, Di Carlo D, Osellame R (2017a) Particle focusing by 3D inertial microfluidics. Microsyst Nanoeng 3:17027–17034
Paiè P, Che J, Di Carlo D (2017b) Effect of reservoir geometry on vortex trapping of cancer cells. Microfluid Nanofluid 21:104
Rana A, Zhang Y, Esfandiari L (2018) Advancements in microfluidic technologies for isolation and early detection of circulating cancer-related biomarkers. Analyst 143:2971–2991
Segre G, Silberberg A (1961) Radial particle displacements in poiseuille flow of suspensions. Nature 189:209–210
Sima F, Sugioka K, Vázquez RM, Osellame R, Kelemen L, Ormos P (2018) Three-dimensional femtosecond laser processing for lab-on-a-chip applications. Nanophotonics 7:613–634
Simon G, Andrade MAB, Reboud J, Marques-Hueso J, Desmulliez MPY, Cooper JM, Riehle MO, Bernassau AL (2017) Particle separation by phase modulated surface acoustic waves. Biomicrofluidics 11:054115
Sollier E, Go D, Che J, Gossett DR, O'Byrne S, Weaver WM, Kummer N, Rettig M, Goldman J, Nickols N, McCloskey S, Kulkarni RP, Di Carlo D (2014) Size-selective collection of circulating tumor cells using vortex technology. Lab Chip 14:63–77
Trotta G, Vázquez RM, Volpe A, Modica F, Ancona A, Fassi I, Osellame R (2018) Disposable optical stretcher fabricated by microinjection moulding. Micromachines 9:388–400
Vázquez RM, Trotta G, Volpe A, Bernava G, Basile V, Paturzo M, Ferraro P, Ancona A, Fassi I, Osellame R (2017) Rapid prototyping of plastic lab-on-a-chip by femtosecond laser micromachining and removable insert microinjection molding. Micromachines 8:328–336
Volpe A, Paiè P, Ancona A, Osellame R, Lugarà PM, Pascazio G (2017) A computational approach to the characterization of a microfluidic device for continuous size-based inertial sorting. J Phys D Appl Phys 50:255601
Vona G, Sabile A, Louha M, Sitruk V, Romana S, Schütze K, Capron F, Franco D, Pazzagli M, Vekemans M et al (2000) Isolation by size of epithelial tumor cells: a new method for the immunomorphological and molecular characterization of circulating tumor cells. Am J Pathol 156:57–63
Wang X, Papautsky I (2015) Size-based microfluidic multimodal microparticle sorter. Lab Chip 15:1350–1359
Wang X, Zandi M, Ho CC, Kaval N, Papautsky I (2015) Single stream inertial focusing in a straight microchannel. Lab Chip 15:1812–1821
Wu Z, Chen Y, Wang M, Chung AJ (2016) Continuous inertial microparticle and blood cell separation in straight channels with local microstructures. Lab Chip 16:532–542
Yamada M, Nakashima M, Seki M (2004) Pinched flow fractionation: continuous size separation of particles utilizing a laminar flow profile in a pinched microchannel. Anal Chem 76:5465–5471
Zhang J, Li W, Li M, Alici G, Nguyen N (2014a) Particle inertial focusing and its mechanism in a serpentine microchannel. Microfluid Nanofluid 17:305–316
Zhang J, Yan S, Sluyter R, Li W, Alici G, Nguyen NT (2014b) Inertial particle separation by differential equilibrium positions in a symmetrical serpentine micro-channel. Sci Rep 4:4527–4535
Zhang J, Yan S, Yuan D, Alici G, Nguyen N, Warkianic ME, Li W (2016) Fundamentals and applications of inertial microfluidics: a review. Lab Chip 16:10–34